Structural Engineering and Mechanics, *Vol. 70, No. 2 (2019) 153-168*
DOI: https://doi.org/10.12989/sem.2019.70.2.153

Study of the effect of varying shapes of holes in energy absorption characteristics on aluminium circular windowed tubes under quasi-static loading

Baaskaran N*[1], Ponappa K[1a] and Shankar S[2b]

[1]*Department of Mechanical Engineering, Kongu Engineering College, Erode, Tamilnadu, India*
[2]*Department of Mechatronics Engineering, Kongu Engineering College, Erode, Tamilnadu, India*

(Received August 7, 2018, Revised February 5, 2019, Accepted February 20, 2019)

Abstract. In this paper, energy absorption characteristics of circular windowed tubes with different section shapes (circular, ellipse, square, hexagon, polygon and pentagon) are investigated numerically and experimentally. The tube possesses the same material, thickness, height, volume and average cross sectional area which are subjected under axial and oblique quasi-static loading conditions. Numerical model was constructed with FE code ABAQUS/Explicit, the obtained outcome of simulation is in good matching with the experimental data. The energy absorbed, specific energy absorption, crash force efficiency, peak and mean loads along with the collapse modes with their initiation point of simple and windowed tubes were evaluated. The technique for order of preference by similarity ideal solution (TOPSIS) approach was employed for assessing their overall crushing performances. The obtained results confirm that efficacy of crash force indicators have improved by introducing windows and tubes with pentagonal and circular windows achieves the maximum ranking about 0.528 and 0.517, it clearly reveals the above are best window shapes.

Keywords: windowed tubes; quasi-static loading; collapse modes; crash force indicators

1. Introduction

Evaluating various methods of energy absorbers or energy dissipating systems, in view of reduction in injuries and damages is one of the prime focused research areas, which has experienced significant attention over the past few decades. Tubular structures have a significant capability of sustaining recommended loads and depleting the energy levels occurred during plastic deformations which are employed as energy absorbing devices widely in various fields namely aerospace, automotive, train and marine structures (Johnson 1978, Cheng *et al*. 2006, Marzbanrad *et al*. 2009, Estrada *et al.* 2017). Normally, the energy absorbers should display higher energy absorption (EA) and minimum peak force (Pmin) usually occurs in axial and oblique loading pattern due to the progressive collapse in nature. The specific energy absorption (SEA) and crash force efficiency (CFE) are also incurred to envisage the effectiveness of tubular structures (Lee *et al.* 2011, Baaskaran *et al*. 2017, Nikkhah *et al*. 2017).

The load carrying capability of tubular structures experiencing under axial and oblique is largely dependent upon the magnitude of the applied load, the shape of geometric discontinuities and implied boundary condition (DeRuntz and Hodge 1963, Morris 1971, Ferdynus 2013, An *et al*. 2015). The wide range of options is available for the design of tubular structure as energy absorbers. They may be flattened, indented or bent under transverse loading pattern, made to split, turned inside out or outside in or expand (Altenhof *et al*. 2005). From the evaluation of various possible designs, the axial and oblique crushing of the tubular members is one of the loading patterns. The overall crushing pattern comprises of three stages. Initially, the compressive force climbs to the initial peak to compensate the resistance offered by the tube. Secondly, the force dips down and fluctuates as far as the crushing progresses. Thirdly, steep increase in the force instantaneously to the corresponding smaller increment in the displacement, which shows the completion of loading process (Børvik *et al*. 2003, Wu *et al.* 2017). The required characteristic of effective energy absorber should exhibit relatively longer stroke with a quite stable reactive force throughout the complete crushing force. Moreover, plastic deformation is experienced over the entire part of the tubular member results in effective utilization for energy dissipation (Eboreime *et al*. 2018, Huang *et al.* 2002, Wang *et al*. 2015). Over the few decades many research efforts have been made to figure out the collapse behavior of circular, square/rectangular tubes subjected under static and dynamic loading. They carried out the theoretical and experimental studies, followed by the numerical simulations due to the advancement in finite element method.

The stabilized energy absorption achieved by the

*Corresponding author, Assistant Professor
E-mail: baaskararcher@kongu.ac.in
[a]Associate Professor
E-mail: ponappa@kongu.ac.in
[b]Professor
E-mail: shankar@kongu.ac.in

http://www.techno-press.com/journals/sem&subpage=7
ISSN: 1225-4568 (Print), 1598-6217 (Online)

introduction of geometric discontinuities, patterned windows (or) triggers which acts as crush initiators during the real impact scenarios. Normally, these types of triggers were fabricated at the required positions at the extreme end where the impactor makes the contact with the tubular structure. It propagates a stable collapse process, initiated nearer to the weak spot without exerting the larger peak forces at the initial collapse fold. It also provokes the expected collapse mode pattern without overlying the larger forces which may result in global bending of the tubular structures. It also increases the overall stability of the structure by facilitating the collapse process at the moving end of the striker and progresses towards the moving end. The larger energy absorption is achieved by the progressive collapse mode of the tubes over the entire span without global bending.

Although, the conventional energy absorbers of circular and square/rectangular members are still of research interests, researchers put more efforts on their topological modifications in view of achieving higher SEA (Chen and Wierzbicki 2001, Estrada *et al*. 2016). In the present scenario the investigation on windowed tubes (i.e., tubes with patterned holes) reveals the significant increase in crash force indicators (Zhang *et al.* 2006). The windowed square tubes under axial crushing showed that initial peak load reduction up to 63% and SEA increment about 54%. The axial crushing test and simulation of windowed tubes of oblique loading were conducted by (Song *et al*. 2013, Qiu *et al.* 2015). The results exhibit the impact of size of windows at various locations, in which the windowed tubes experiences higher energy absorbing capability at larger load angles. Followed by energy absorption pattern in smaller load angles of windowed tubes was much similar to the simple tube and also size of the windows was determined by the proposed algorithm (Hwang *et al.* 1993, Song *et al.* 2012). The double and triple cell square tubes experiences 15% higher SEA than the conventional single cell tube. The increase of 50% in SEA by dividing the cross section of 3×3 pattern cells is demonstrated and proposed a new multi cell profile which shows the 190% increase in SEA when compared to the single cell (Kim 2002). The methods of subdividing circular tubes by non-deformable discs exhibits the increase of 21% SEA par to the comparison of circular tubes (Abdul-Latif, Ahmed-Ali *et al*. 2017). The quasi-static axial compression testing on square tube extruded aluminium alloy with and without presence of discontinuities of circular shape located in the middle of the tube. The obtained results clearly notifies that reduction of peak crush force was about 5.2-18.7% by incorporating the through-hole crash initiator, also increase in the range of 26.6-74.6% of total energy absorption was experienced (Arnold and Altenhof 2004). The axial quasi-static crushing of circular and square tubes with the presence of circular discontinuities using the LS-DYNA explicit FE-code were studied. The observation shows the good correlation between the results obtained between the numerical and experimental model (Mamalis *et al.* 2004).

The introduction of cut-outs in tapered TW tubes results in increase the efficacy in overall crashworthiness characteristics (Guler *et al.* 2010) and (Taştan *et al.* 2016) drastic increase in specific Energy Absorption (SEA) about 26.4% and Crash Force Efficiency (CFE) about 27.4% for frusta tubes containing cut-outs than the normal tubes. The crushing response of tubular structures such as simple tubes (with no windows) and windowed tubes (with various profiles) are subjected to both axial and oblique loading conditions. The FEA model were developed and properly validated by conducting the experimental results. The observed results revealed that the axial collapse experienced for all the tubes, the collapse pattern for simple tubes is of extensional mode (θ=0°) followed by the windowed tubes experiencing the symmetrical mode. The presence of transverse inertia effect caused due to dynamic loading leads to the occurrence of extensional mode collapse pattern for simple tubes. Also, the square tubes experiencing the collapse mode of symmetric during quasi-static loading, observes the change in collapse mode pattern of extensional mode when subjected to dynamic loading (Altin *et al*. 2018).

So far, pattern design on tubular structures received larger attention. Initial feature or pattern is knowingly introduced on the tubular member to obtain the high energy absorption capability. More studies show that the stabilization of crushing process was achieved by introducing feature or pattern in the tubes (Gautam and Dixit 2012). In turn, it provokes the prediction and control of collapse mode is possible. The effect of longitudinal grooves in the square tubes shows the increase of SEA about 83% in the numerical investigation (Morris 1971, Zhang *et al.* 2006). The numerical study on the patterned square tubes experienced 28% of SEA increase than the conventional tube (Zhang *et al.* 2006). It was mainly due to the triggering action which results in the formation of extensional mode. From the above, the improvisation of SEA can be possibly done by introducing pattern in the tubular member (Song *et al*. 2013). Till now pattern design has more focused on varying the geometrical shape of the tube with the existing or slight increase in total mass. The mass reduction is more crucial in designing certain type of applications (Huang *et al*. 2002) (i.e., design of planetary landing probes in the aircraft landing gear, where it is used as energy dissipation device in which its overall weight to be minimized in view of more utilization in payloads). Although, previous works are much focused on determining the shape and size of the components in which it includes patterning, grooving and corrugation with origami. (Zhang *et al.* 2006, Auersvaldt and Alves 2014) conducted investigation on windowed square and hexagonal tubes subjected to impact loading. The obtained results revealed that higher SEA and significant reduction in initial peak force is achieved for square windowed tubes compare to the simple tubes (Ghamarian *et al.* 2013).

Current works on windowed tubes are mainly focused on circular or rectangular holes. In this paper, quasi-static crushing behavior of thin walled circular tubes with different shapes of geometric discontinuities under axial and oblique loading are studied experimentally and numerically. The MCDM method TOPSIS is employed to assess the overall performances under different loading conditions. The significance of this method is the evaluation

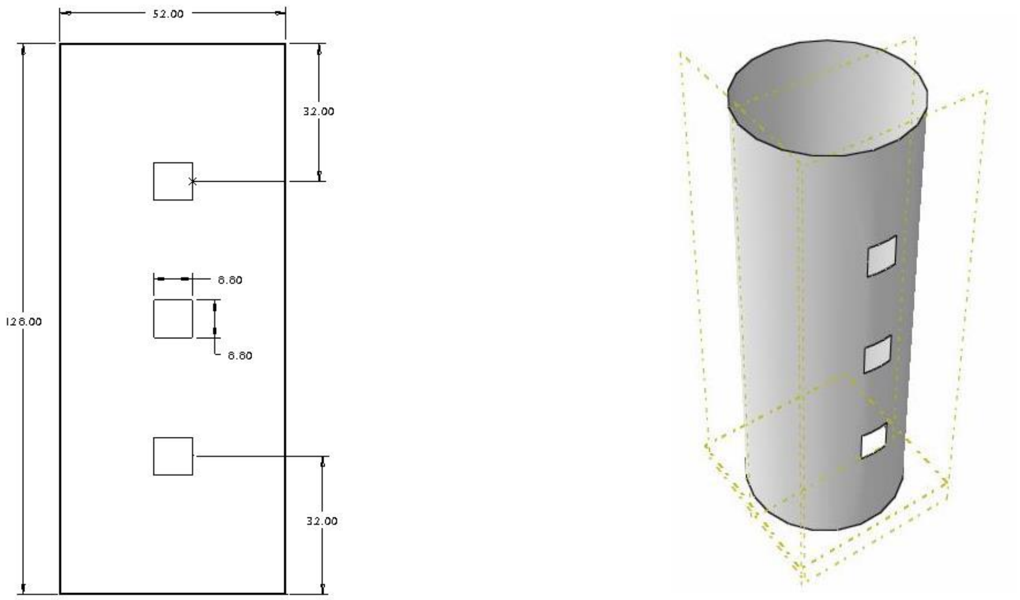

Fig. 1 Geometry of the patterned tubes with circular holes (mm)

of multiple criteria with their available options and ranking the options based on their achieved score. The workflow of this paper is arranged as follows. Initially the geometries of the windowed tubes are exhibited. Experimental tests were performed to validate the numerical procedure which was carried out by ABAQUS/Explicit. The obtained numerical results of different windowed tubes subjected under various loading conditions on crush force indicators are analyzed and their performances are ranked by TOPSIS method.

2. Geometry and materials

All the tubes considered are of circular cross sections, with length being 128 mm, diameter being 52 mm and wall thickness being 0.0072 mm. The geometry of the patterned tubes with circular holes is shown in Fig. 1. There are three holes on the outer peripheral area in which the line of axis of each hole is maintained in the straight line. In our present case, the thin-cylindrical shells were examined for energy absorption characteristics. The determination of arriving appropriate diameter for the circular cut-outs which should be engraved on the cylindrical shell is normally based on the governing equation presented by (Toda 1983). The ultimate buckling behavior of cylindrical members possessing symmetric cut-outs subjected to axial compression loading were governed by the equation

$$\propto = \frac{a}{\sqrt{Rt}} \tag{1}$$

Where a indicates the radius of the hole, R and t indicates the radius and thickness of the cylinder. The effect on presence of cut-outs is negligible when the $\propto$ value is approximately 1.0. The position of $\propto$ value positioned between 1.0 and 2.0, experiences mild reduction in buckling loads. Also, buckling loads experiences prolonged reduction for the values of $\propto$ higher than approximately 8.0. Here the $\propto$ value is maintained below 5.0 for the single cut-outs, in turn it is reliable that the chosen diameter had no significant effect in reducing the buckling loads. The holes are positioned at equal distance on the surface of the wall, having the different configurations maintaining the cross-sectional area of 78.53 mm^2. The elapsed distance between the center of the top (bottom) and the top (bottom) of the tube is 32 mm. The linear distance between the lines of axis to the left or right exterior end of the tube is being fixed as 26 mm. The same pattern for window arrangement is followed invariably for all the different shapes of holes same as the circular hole. The Fig. 2 represents the geometric description of simple tubes without windows and windowed tubes considered in experimental and as well numerical simulation. The material used in this study is aluminium 2024 alloy which is normally chosen as energy absorbers due to their lower weights. The material parameters are as follows: Young's modulus E=69000 Mpa and Poisson's ratio v=0.35, plasticity models are given in the Table 1, where ASTM-B-209 standard were utilized to extract the material parameters (Lesuer 1999, Palanivelu *et al*. 2011). While modeling the impact scenarios, it is essential to include the stain rate and temperature effects and its implication on flow stress. The most developed plasticity models which are more appropriate for large strain rate during deformation, it also envisages the effect of strain rate and temperature on occurred deformation.

$$\sigma_T = \left[A + B(\varepsilon_{eff}^p)^N\right]\left(1 + C\ln\frac{\dot{\varepsilon}_{eff}^p}{\dot{\varepsilon}_0}\right)\left[1 - \left(\frac{T - T_0}{T_m - T_0}\right)^m\right] \tag{2}$$

Here (σ_T) represents the dynamic flow stress followed by effective plastic strain as $(\varepsilon_{\mathrm{eff}}^{\mathrm{p}})$, reference strain rate as $(\dot{\varepsilon}_0)$. Also followed by the material parameters (A, B, N, M and C) which represents the initial yield stress, hardening modulus, strain rate dependency coefficient, work-hardening exponent and thermal softening component. (T_m) and (T_0) represents the melting temperature and

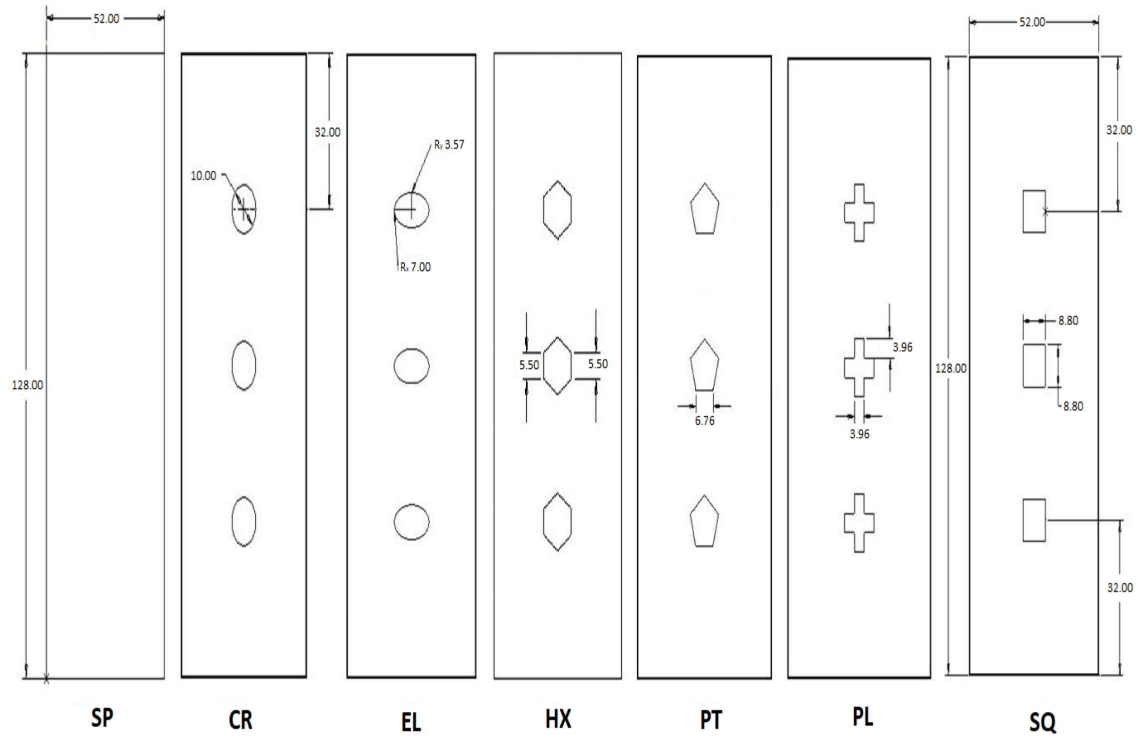

Fig. 2 Geometric description of simple and all patterned tubes (mm)

Table 1 The material parameters

	Johnson-Cook material parameters					Cowper-Symonds Parameters				
Material	Density (kg/m^3)	A (MPa)	B (MPa)	C_p (J/kg K)	T_{melt} (K)	n	c	m	C(S^{-1})	P
Al 2024	2770	265	426	875	775	0.34	0.015	1.0	6500	4

*T_{melt}=melting temperature; C_P=Sp. Heat capacity; A, B, n, c, m, C and P are material constants

Transition temperature. The significance of transition temperature lies in neglecting the dependence of temperature while expressing the yield stress and it is normally assumed of 297 K at the room temperature.

3. Experiment

3.1 Specimens

Schematic view of the fabricated windowed tubes is shown in Fig. 3. The experiments were conducted on the prepared specimens.

3.2 Mounting of the specimens

The thickness of the windowed tubes is very minimal on par compared with the length of the tube. Due to its minimum thickness if it is directly loaded in the experimental set up, there is the possibility of shift in line of axis and edge perforation. To avoid the above special type of fixture arrangement is fabricated and sequence of steps is followed to mount the specimen in the fixture. To minimize the stresses that developed during mounting of the specimen to be done on the lathe machine. Although, the keen observation is maintained to ensure the end faces of bottom and top flanges of the mounting fixture were parallel. The interior portion top mounting flange is accommodated in the headstock and bottom mounting flange along with the taper was inserted in tailstock. Followed by careful insertion of inner part of bottom and top flanges which to be aligned with spindle axis. Finally, 12 (M6) screws were used to fasten the mounting flanges with the specimen and transition fit is achieved between the specimen and the mounting flanges of both top and bottom which is graphically illustrated in Fig. 4. Then the specimen is released from the headstock and tailstock which is to be ready to be placed in loading machine (Eboreime *et al*. 2018).

3.3 Experimental procedure

The experimental setup is shown in Fig. 4 (Baaskaran *et al*. 2018). Different quasi-static crushing of specimen is performed on the patterned tubes to mitigate their behavioral change when subjected to axial crushing (Fan *et al*. 2013).

Three samples of each configuration were tested and mean value is attained for the final result, in view of achieving higher accuracy. The specimen is then

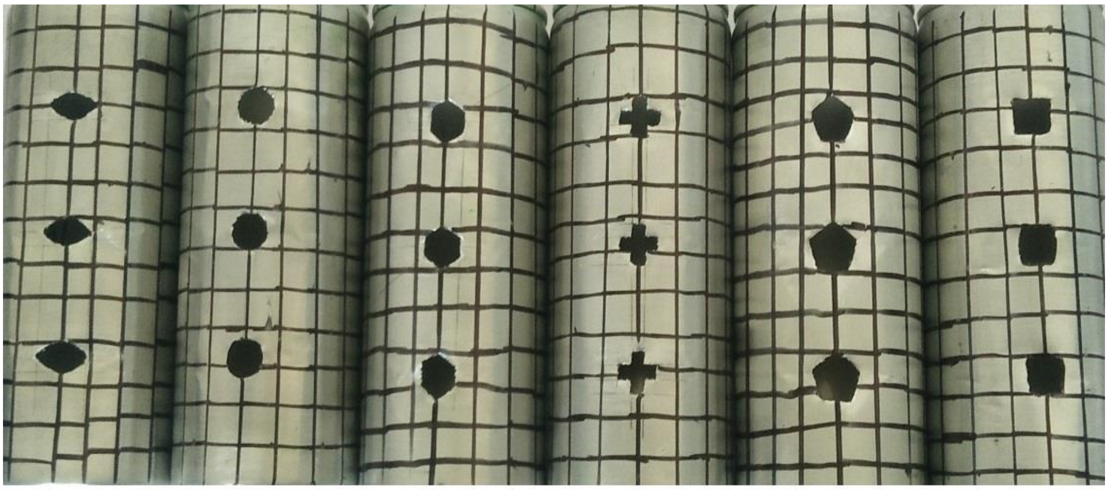

EL CR HX PL PT SQ

Fig. 3 Fabricated specimen for all the patterned tubes

(a) Deepak DTRX apparatus

(b) Mounting Fixture

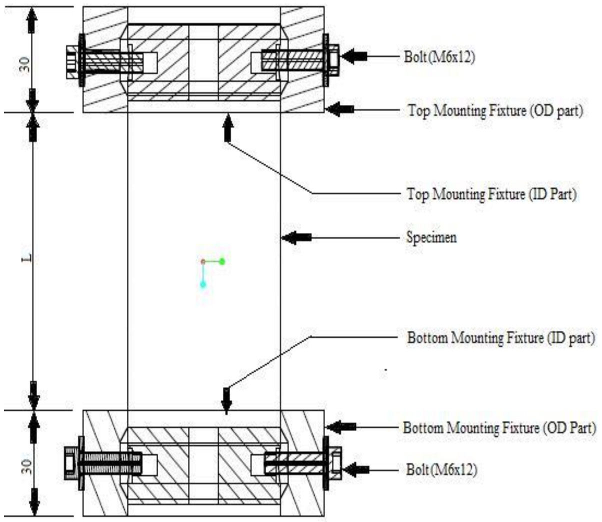

(c) Cross sectional view of mounting fixture

Fig. 4 Experimental set-up with accessories (Baaskaran *et al*. 2018)

subjected to quasi-static crushing. DEEPAK (DTRX) hydraulic machine is equipped with 30 kN load cell which was utilized for quasi-static axial compression tests. The calibration of the machine is done periodically, there is the

Table 2 The Experimental results for various specimens under quasi-static loading at 0° AOI

Specimen code	EA (J)	P_{mean} (N)	P_{max} (N)	CFE (%)	SEA (J/kg)	Collapse starting point	Collapse mode
SP	7.949	90.55	547	16.55	27495.67	MOS	D
CR	4.246	49.22	398	12.36	14686.95	ME	D
EL	5.235	66.72	399	16.72	18107.92	ME	D
SQ	5.575	63.94	530	12.06	19283.98	MOS	D
HX	5.837	70.31	453	15.52	20190.24	MOS	D
PL	5.568	70	466	15.02	19259.77	MOS	C
PT	5.412	70.88	487	14.55	18720.16	MOS	C & D

Table 3 Comparison of results between experiments and simulations at 0° AOI

Specimen code	Difference %					Collapse starting point	Collapse mode
	EA (J)	P_{mean} (N)	P_{max} (N)	CFE (%)	SEA (J/kg)		
SP	-5.16	2.54	-7.64	9.69	-5.065	Similar	Similar
CR	0.6	9.7	4.26	5.67	7.757	Similar	Similar
EL	-9.36	7.26	0.25	7.05	-9.45	Similar	Similar
SQ	7.1	9.1	1.1	8.2	0.688	Similar	Similar
HX	-6.43	8.56	-0.79	9.27	-6.31	Similar	Similar
PL	-5.03	9.6	-0.28	9.8	-5.06	Similar	Similar
PT	-9.2	9.8	1.06	8.5	-9.317	Similar	Similar

presence of two jaws in the machine in which upper one is movable and the lower one is stationary. During the compression tests, the specimens were compressed between upper and lower jaws without any additional restraints. The quasi-static condition is established and to ensure the absence of dynamic effect, the control displacement of specimen at a rate of 5 mm/min until confined crush. It entails complete crushing of specimen with the steep increase in the recorded load. To ensure the absence of dynamic effects while testing, other researchers have applied upper jaw speed between the ranges of 5 to 10 mm/min (Khalkhali *et al*. 2016). In this course, we opt to choose 5 mm/min to ensure the performed tests are within quasi-static range. The crushing loads and displacements were captured by an in-built automatic data acquisition system. The results obtained for the above which is shown in Table 2 is utilized for validation of numerical approach in the forthcoming sections.

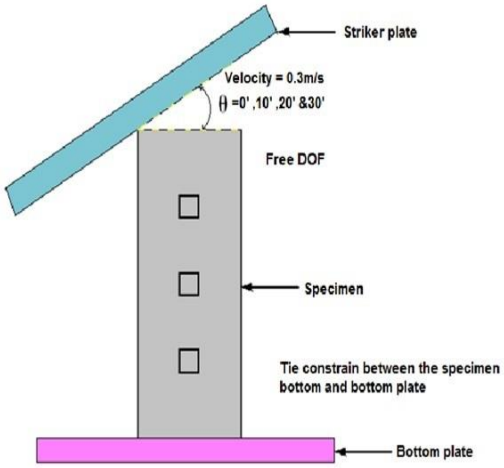

Fig. 5 Finite element analysis set-up for quasi-static loading

4. Modelling and validation

4.1 FE Modeling

FE code ABAQUS/Explicit (ABAQUS 2011) was adopted for the quasi-static axial and oblique loading simulation. The Johnson-cook parameters are utilized to characterize the material behavior which includes the post-yield responses which are depicted in Table 1. The schematic finite element analysis set-up for quasi-static loading is shown in Fig. 5. The bottom flange of the fixture is placed on the base plate and top flange of the fixture is free to accommodate striker plate. The striker plate only moves in transverse direction without rotation about vertical axis. The three-dimensional shell element S4R are chose to model the patterned tube, the mesh refinement along the edges of the windows are performed by advancing front algorithm. The total of 2243 quad dominated element is utilized for free meshing; local seeds of approximate element size of 2.5 mm are used. The striker and base plate were modeled using R3D4 elements. The general contact algorithm with the coefficient of friction 0.2 is employed to create the interaction between the striker and specimen (Dehghan-Manshadi *et al.* 2007, Tarlochan *et al.* 2013). The velocity was applied on the specimen via top striker plate. The loading rate in actual quasi-static process was about 5 mm/min, which were too slow results in increase of time step too much. The artificial ramping velocity of 0.3 m/s is applied on the movable striker, in view of reducing the time step of the process. Similar approach by for controlling velocity by employing AMPLITUDE and SMOOTHSTEP sub option was reported (Khalkhali *et al*. 2016).

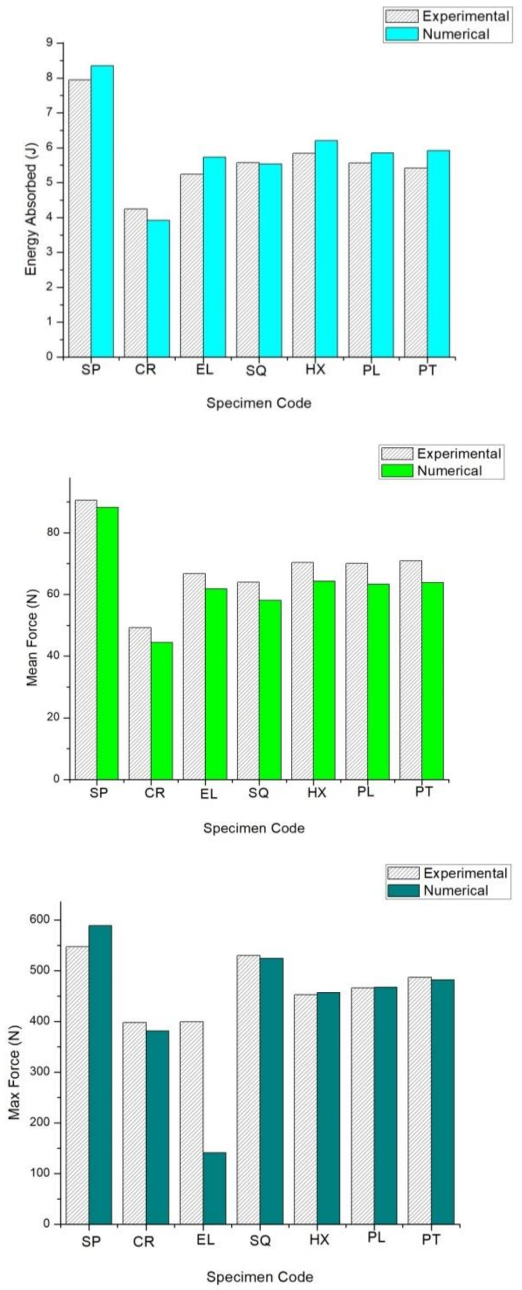

Fig. 6 Comparison between the experimental and numerical results for various crashworthiness indicators

4.2 Structural crashworthiness indices

It is very necessary to predefine the crash indices (CI) to evaluate the crashworthiness. The various parameters involved are energy absorption (EA), mean crushing force (P_{mean}), peak crushing force (P_{max}) are broadly used to estimate the crashworthiness characteristics of thin walled tubes. The EA can be termed as work done by the crushing force in longitudinal deformation (Δ) and for a given structural deformation, it can be given as

$$E_a = \int_0^{\Delta} F.d\Delta \tag{3}$$

The SEA is defined as the ability of energy absorption capability per unit mass of the crushed structural component and given as

$$SEA = \frac{\int_0^{l_{max}} F(l).dl}{M_{bc}} \tag{4}$$

The mean crushing force can be termed as the measure of average forces required to compress the material in form of progressive folding.

$$P_{mean} = \frac{\int_0^{l_{max}} F(l).dl}{l_{max}} \tag{5}$$

The peak crushing force during the quasi-static process can be given as

$$P_{max} = max\ (F(l)) \tag{6}$$

The crash force efficiency is defined as the ratio between the mean and maximum load experienced. Normally, the lower CFE is not preferred because of higher initial force is directly transferred to the mounting structure.

$$CFE = \frac{p_{mean}}{p_{max}} \tag{7}$$

4.3 FE experimental validation

To validate the developed FE model, axial quasi-static crushing experimental test results on patterned tubes with various geometrical discontinuities are compared in Table 3. The maximum variation of results observed is within 10% for various parameters like peak, mean and energy absorption is presented in Table 3. In Fig. 6, the comparison between the experimental and numerical results for various crashworthiness indicators exhibits more similarities. The deformed shapes of simple and windowed tubes obtained in both numerical and experimental are shown in Fig. 7. The result also reveals the presence of minor variation in the starting point and formation of collapse modes in the specimens. It may be due to flawed approximation of friction coefficient in FE modeling. The good agreement in predicting collapse mode, peak force and energy absorption for the simple and patterned tubes under quasi-static loading, which ensures the perseverance of the crushing response extracted form simulation for various patterned tubes.

5. Results and discussion

The thin-walled tubular members normally used for crashworthiness applications which are experiencing both axial and oblique impact loads. The primary function in providing dents (or) patterned on the tubes in view of delaying the buckling characteristics, which also leads to the progressive folding. In our current study the AOI (Angle of inclination) is limited to 30° due to the safety regulations which demands the frontal protection system (bumper) can able to withstand the oblique loads till 30° AOI with respect to the longitudinal axis. The thickness and AOI of the

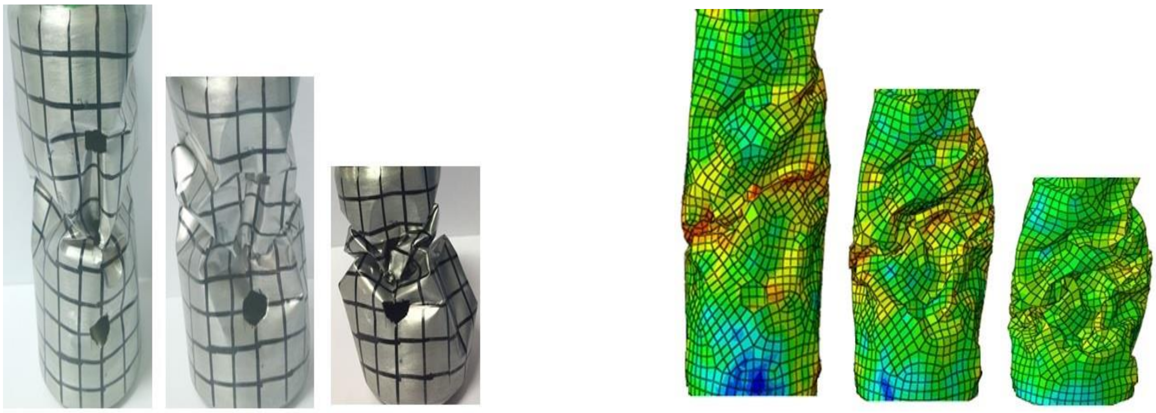

(a) Hexagon

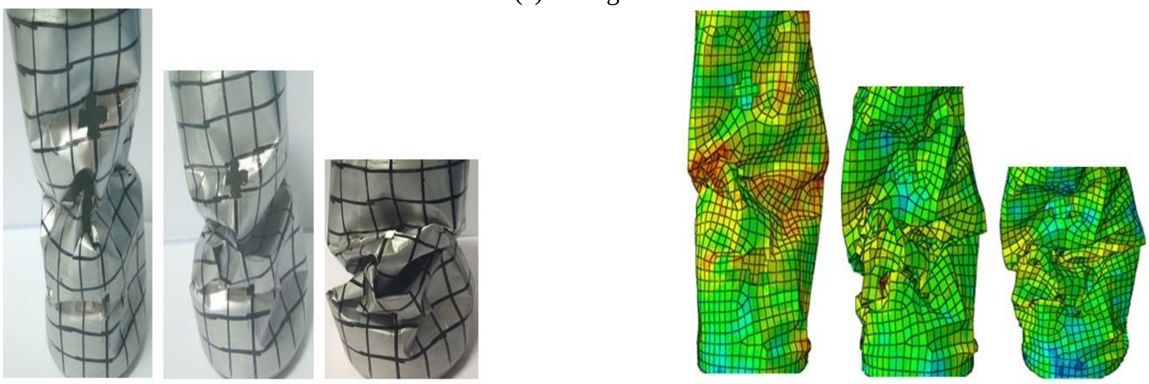

(b) Plus

Fig. 7 Deformed shape of simple and windowed tubes

tubular members were the dominant factor in deciding the occurrence of the collapse mode pattern. Also, the maximum peak force and mean force had drastically reduced by the increase of AOI. Moreover, the variations in collapse mode behavior when the tubular member subjected to quasi-static and dynamic loading cases were not observed. The above behavior clearly indicates that increasing of the oblique loading AOI beyond 30° results in the occurrence of global bending which also drastically reduces the energy absorbing capability. The proximity of experiencing the global bending in tubular structures increases with the increasing of AOI. Also, the buckling characteristics will improvise the reduction in maximum peak force as well as energy absorbing characteristics (Estrada *et al.* 2017).

The collapse modes mapping can be expressed by the letters D, C and (D&C) represents diamond, concertina and (diamond & concertina) respectively. Normally, when the collapse progresses the opposite two faces diagonally bends inwards, also the other two faces bends outwards. Furthermore, the mid-section is completely opened and forms the rhombus shaped structure. The above formation indicates the occurrence of diamond collapse mode. Also, the occurrence of progressive collapse mode symmetrically was normally termed as concertina mode. The simple and circular windowed tubes exhibits completely diamond collapse mode pattern and originated at the mid of specimen. Followed by the elliptical windowed tubes in which the occurrence of collapse mode pattern is completely diamond and initiated at moving end of the striker. The mid of specimen collapse initiation were experienced for square and pentagonal windowed tubes, followed by the diamond and concertina collapse mode for hexagonal and polygonal windowed tubes respectively.

Fig. 8 represents the crushing load-displacement curves of all the simple and patterned window tubes at different load angle. The deformed shape of individual tubes at varied load angles is exhibited in Fig. 9. The collapse modes of the tubes take place axially and the results for all the windowed tubes under simulations at 0°, 10°, 20° and 30° AOI (Angle of inclination) is shown in Table 4.

The deformation of various profiles (SP, CR, EL and HX) experiences complete diamond mode irrespective of all load angles (θ=0°, 10°, 20° and 30°). The mixed mode in which involves both concertina & diamond for the profile (PT) and complete concertina mode is observed for the profile (PL) for all load angles. This phenomenon is already observed in in their experimental tests, in which collapse of circular tubes normally occurs in symmetric or diamond mode under quasi-static loading and experiences extensional mode if it is loaded dynamically or direct impact loading (Langseth and Hopperstad 1997).

The stabilized force can be exerted by the tubular structures, which can be achieved by providing patterns of different geometrical shapes. By facilitating the proper blind spots on the appropriate locations, it enables the tube to undergo the constant progressive folding at the extreme positions without exerting maximum peak forces during the

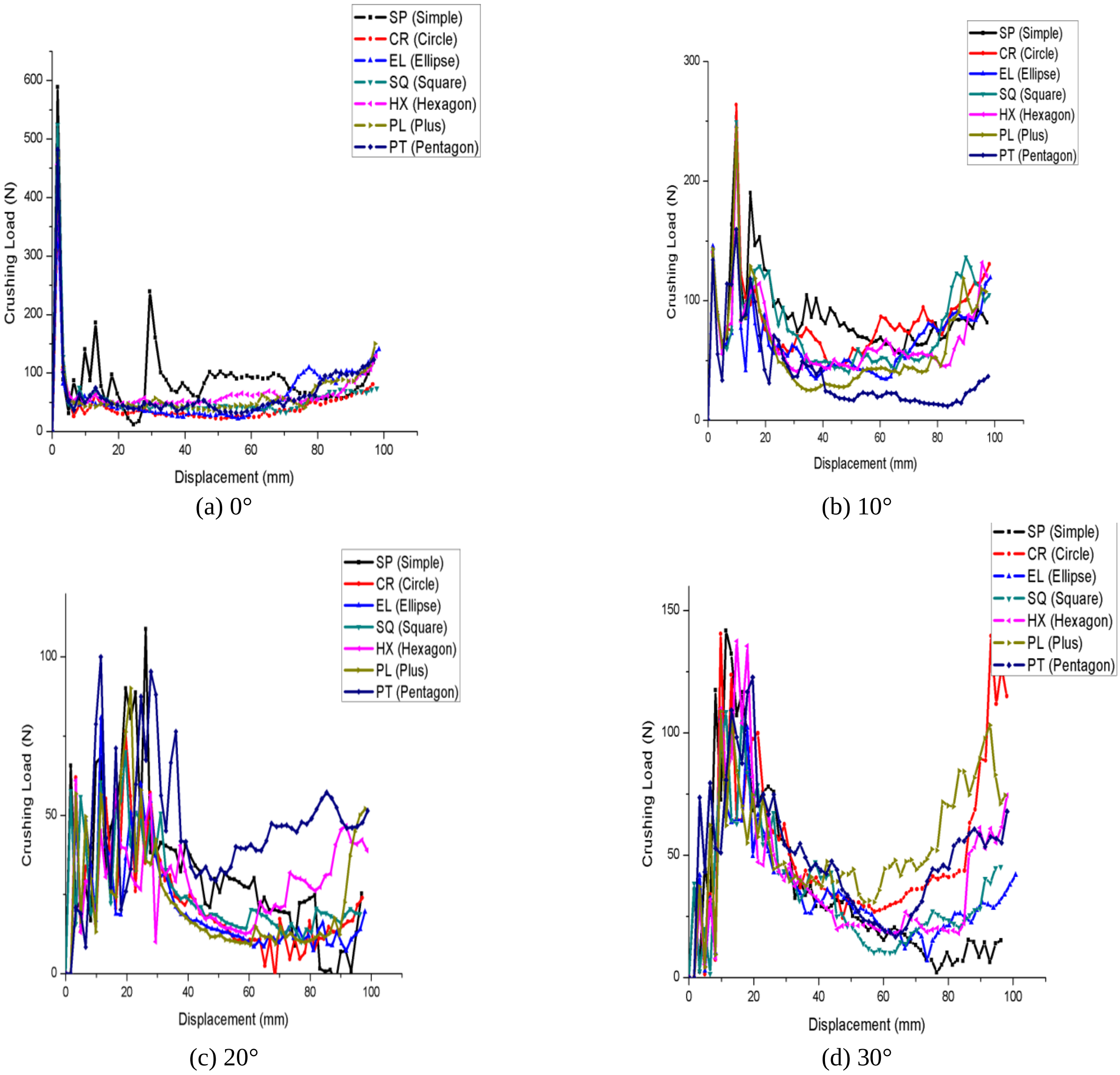

Fig. 8 Load-displacement curve for simple and windowed tubes at all load angles

first fold.

The dynamic response and energy absorption capability of the windowed tubes which is loaded laterally and obliquely were initially compared by altering the load angle. The structural crashworthiness indices such as energy absorbed, specific energy absorption, crash force efficiency, maximum peak force were presented in Fig. 10 in view of evaluating the crashworthiness. It is observed that maximum peak forces of patterned tubes are comparatively lesser than the simple ones. The above case clearly indicates that the patterned windowed tubes exerts lesser initial peak forces, the reason lies beneath were that lowering the resistance exerted by the tubes when it is experiencing the axial crushing forces. The introduction of geometric discontinuities, lower the initial resistance as well as higher energy absorption and provide fairly uniform response. The reduction in maximum peak force also resulted in reduction in EA. The elliptical and circular windowed tubes exhibited minimum peak forces irrespective of all loading angles.

The magnitude of the crashworthiness indices were substantially lowered by increasing the angle of inclination (AOI) beyond 20° which were irrespective for all the patterned tubes. Also, the energy absorbing capabilities were also reduced because of the lateral movement of the striker pushes the tube away from the central axis resulting in a global bending collapse mode. However, the formation of the progressive collapse mode pattern and resistance offered by the tubes were greatly reduced. Also, the maximum peak force can also be altered by the width of the patterned window. The wider in the pattern width, the larger in reduction of peak force which also agrees with the experimental work. The circular windowed tube experiences the minimum peak force comparatively to other profiles. The aspect ratio of the triggering elements plays the significant factor in determining the collapse mode pattern and crashworthiness indicators (Ferdynus *et al*. 2018).

Followed by the energy absorption in which simple tube exerts higher EA than those of windowed tubes except at 20° and 30°, also the largest EA experienced by patterned

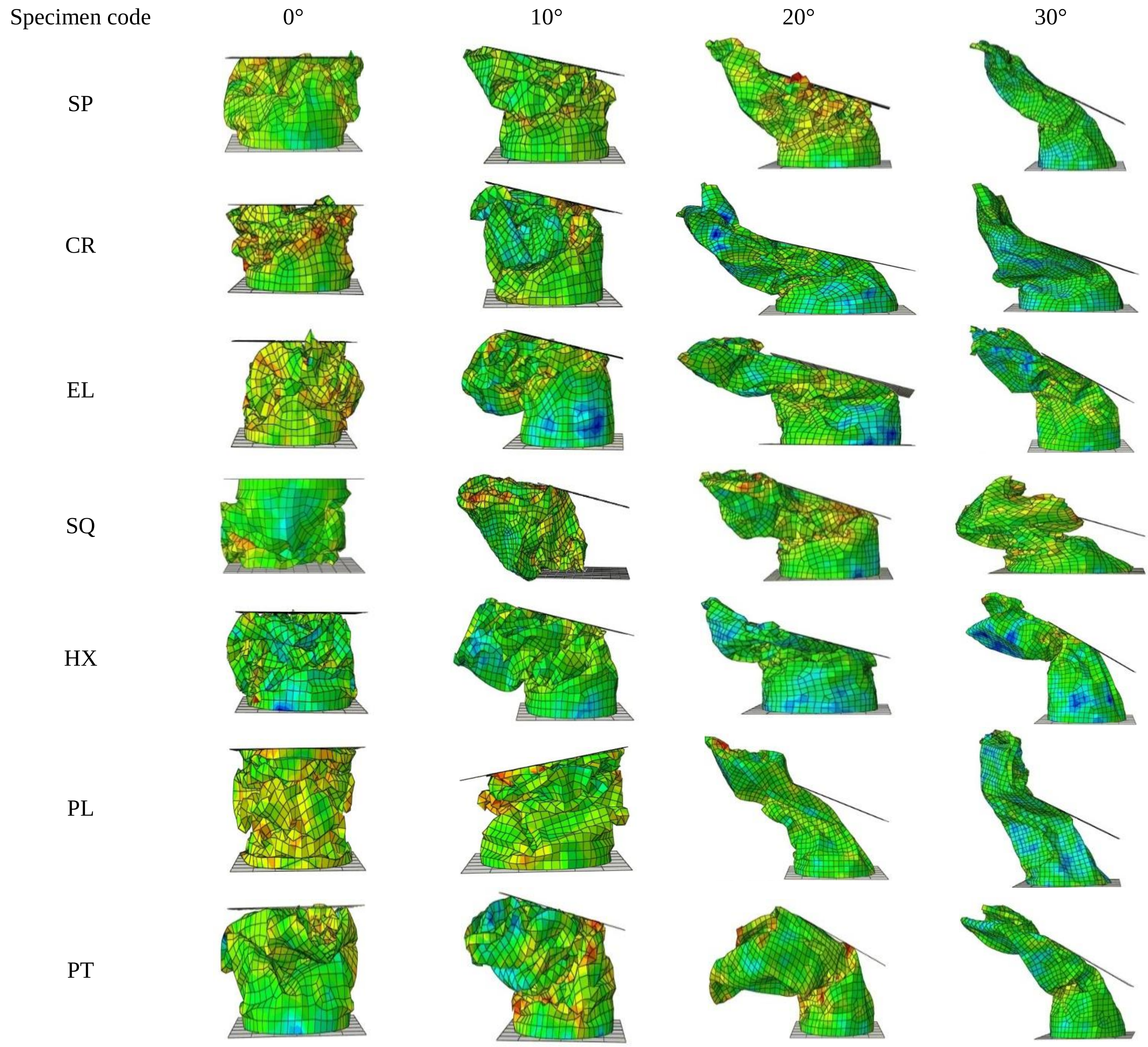

Fig. 9 The deformed shape of individual tubes with specimen codes at varied load angles

tubes with circular holes at a load angle of 10° which was observed earlier in (Nikkhah *et al*. 2017).

Patterned window tubes with circular and pentagonal holes experiences higher crash force efficiency than simple tubes except 0˚ at all the load angle patterns. The lowest CFE is recorded under axial loading is about 11.07 for square tubes and the highest being 15.53 for the Ellipse-hole profile tube. It is evident that lesser CFE is achieved in axial loading (θ=0°) due to the formation of progressive diamond collapse mode provokes high peak (P_{max}) load carrying capacity on par compare to the mean load (P_{mean}). The contrast becomes larger when the tubes are subjected to oblique loading. Although, if the angle of oblique loading exceeds beyond (θ=20°) also shows reduction in CFE for the profiles CR, EL, PL tube.

It is evident that only increase in oblique angle does not provide higher CFE is clearly visible, the reason lies beneath was load carrying capacity is completely reduced due to the absence of progressive folding pattern. At (θ=20°) all the windowed tubes shows higher CFE than the simple profile tube. On SEA, simple tube shows better response than the patterned tubes for all the load angles at (θ=0° and 10°), where polygonal and hexagonal tubes exhibits higher SEA at (θ=20° and 30°). On considering only the windowed tubes, those with hexagonal holes possess consistent largest EA except at (θ=20° and 30°) followed by the polygonal hole tubes at (θ=20°) and pentagonal hole tubes at (θ=30°). For those showing least EA than hexagonal holed tubes, e.g., polygonal and pentagonal holed tubes exhibits similar pattern of energy absorption irrespective of load angles. Comparing only hexagonal and polygonal hole tubes, it is visible that hexagonal hole tube gives better than polygonal hole tubes in EA at all load angles except at (θ=20°). On comparing the whole, ellipse profile tube shows lowest EA irrespective of all load angles except at (θ=10˚).

Table 4 Results for all the windowed tubes under simulations at 0°, 10°, 20° and 30° AOI

Specimen code & AOI	EA (J)	Pmean (N)	Pmax (N)	CFE (%)	SEA (J/kg)	Collapse starting point	Collapse mode
				SP			
0°	8.35	88.25	588.84	14.99	28888.35	MOS	D
10°	8.44	87.92	253.44	34.69	29178.77	MOS	D
20°	3.46	36.48	141.81	25.73	11954.47	MOS	D
30°	3.08	31.88	108.86	29.29	10644.30	MOS	D
				CR			
0°	3.92	44.44	381.01	11.66	13547.63	ME	D
10°	7.68	81.12	139.68	58.08	26567.41	MOS	D
20°	4.77	52.66	139.61	37.72	16492.29	MOS	D
30°	2.12	22.55	76.51	29.47	7323.08	MOS	D
				EL			
0°	5.73	61.87	398.19	15.54	19819.82	ME	D
10°	6.29	66.69	145.65	45.79	21769.25	ME	D
20°	3.24	33.19	106.11	31.28	11212.96	ME	D
30°	2.02	20.80	80.80	25.75	6993.63	ME	D
				SQ			
0°	5.54	58.08	524.28	11.08	19151.29	MOS	D
10°	7.36	77.20	249.54	30.94	25466.91	MOS	C
20°	3.38	35.42	108.56	32.63	11707.36	MOS	D
30°	2.55	26.04	70.06	37.17	8821.62	MOS	C
				HX			
0°	6.21	64.29	456.60	14.08	21464.49	MOS	D
10°	6.23	67.17	140.92	47.66	21561.46	ME	D
20°	3.72	40.16	137.48	29.21	12869.30	MOS	D
30°	2.70	28.20	61.01	46.22	9329.81	MOS	D
				PL			
0°	5.85	63.29	467.35	13.54	20235.13	MOS	C
10°	5.72	61.57	244.68	25.16	19769.82	MOS	C
20°	5.08	54.50	108.78	50.10	17586.90	MOS	C
30°	2.23	24.02	90.13	26.65	7709.08	ME	C
				PT			
0°	5.92	63.90	481.83	13.26	20464.33	MOS	D & C
10°	3.79	39.21	134.07	29.24	13115.72	MOS	D & C
20°	4.77	49.88	122.76	40.64	16505.96	MOS	D & C
30°	4.38	45.28	100.02	45.27	15152.23	MOS	D & C

*MOS-Mid of specimen, ME-Moving End, D-Diamond, C-Concertina

The initial peak force of circular holed tube shows more consistent, irrespective of the loading angles. Windowed tubes with square holes experiences highest initial peak force at (θ=0° and 10°). Moreover, it achieves highest initial peak force among the windowed tubes when it is subjected to axial loading. The circular hole tube shows the maximum peak force at an angle (θ=20°), followed by pentagonal hole tube at an loading angle of (θ=30°). The consistencies in energy absorption rate were effective for the profile (PT) on comparing with circular profiles.

It also witnessed that the maximum peak forces were obtained for pentagonal profiles involving all loading angles with the maximum value of 481.83 N at (θ=0°) under direct loading. Similarly, for the same loading condition the circular profiles exhibits the maximum value of 381.01 N. Although, the same cross-sectional area were utilized in fabrication of windowed tubes experiences notable variations in crashworthiness indicators.

The circular profile possesses maximum width when comparing on par with the pentagonal profile. The reason

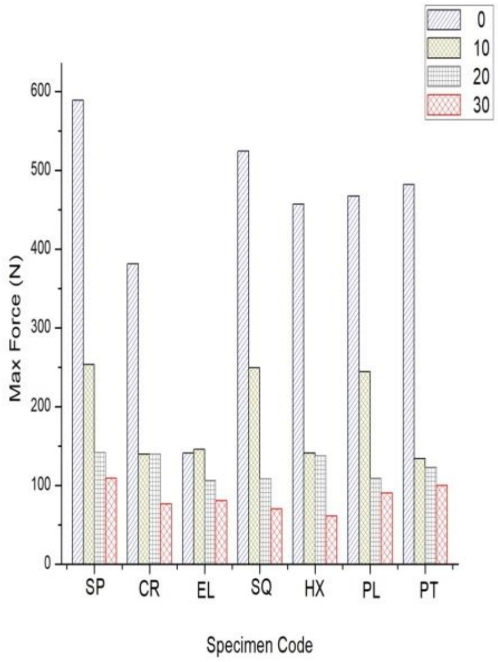

(a) Max Force

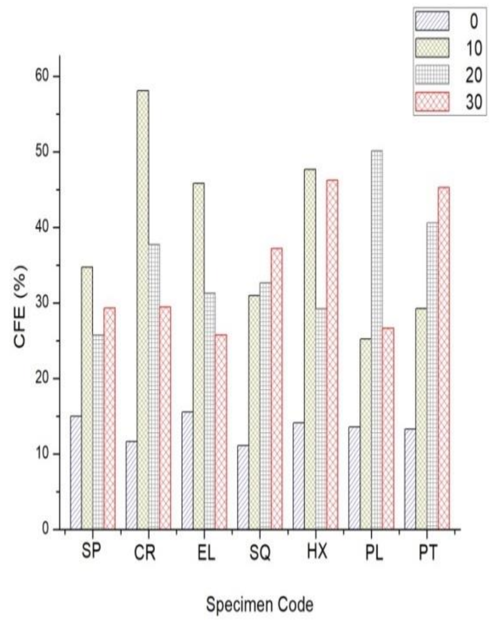

(b) Crash force efficiency

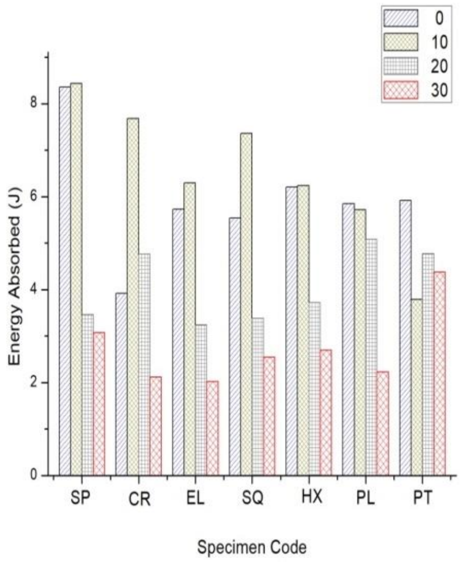

(c) Energy absorbed

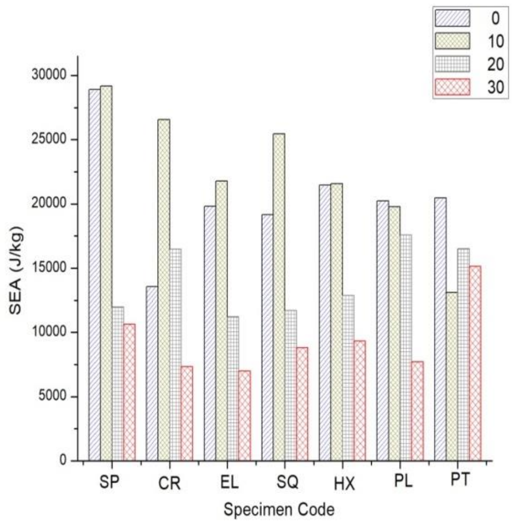

(d) Specific energy absorption

Fig. 10 The analogy of windowed tubes at varied load angles

lies beneath in this mechanism were that the increase in width of the window drastically reduces the maximum peak forces. Furthermore, by maximizing the width of the profile provokes the presence of minimum material in the circumferential direction when subjected to the direct loading i.e., (θ=0°). Also, there is no much difference between both the profiles in oblique loading i.e., (θ>0°). The diamond collapse mode is observed for CR profiles for all AOI and the origin of collapse starting point is at the mid of the specimen (MOS) for all cases except direct loading where it experiences at the moving end. The observation of diamond and concertina (D&C) collapse mode with the origin at the mid of the specimen (MOS) had been observed for pentagonal profile tubes experiencing at all loading cases.

The above are the notable differences that can be visible in assessing the crashworthiness indices. It is evident that from Fig. 9 shows that the windowed holes crushing performance vary under different loading condition. The TOPSIS method was employed by considering maximum load (P_{max}), energy absorbed (EA) and crash force efficiency (CFE), in order to compare the overall performance of all the patterned tubes subjected under different loading conditions. The same weightage is to be assumed for all the criterions, procedures and results elaborated in upcoming sections.

Table 5 Evaluation matrix extracted for all the windowed tubes under simulations at 0˚, 10 ˚, 20˚ and 30˚ AOI

CI	Pmax (N)	EA (J)	CFE (%)	Pmax (N)	EA (J)	CFE (%)	Pmax (N)	EA (J)	CFE (%)	Pmax (N)	EA (J)	CFE (%)
Sp.code		0°			10°			20°			30°	
SP	588.84	8.35	14.99	253.44	8.44	34.69	141.81	3.46	25.73	108.86	3.08	29.29
CR	381.01	3.92	11.66	139.68	7.68	58.08	139.61	4.77	37.72	76.51	2.12	29.47
EL	398.19	5.73	15.54	145.65	6.29	45.79	106.11	3.24	31.28	80.80	2.02	25.75
SQ	524.28	5.54	11.08	249.54	7.36	30.94	108.56	3.38	32.63	70.06	2.55	37.17
HX	456.60	6.21	14.08	140.92	6.23	47.66	137.48	3.72	29.21	61.01	2.70	46.22
PL	467.35	5.85	13.54	244.68	5.72	25.16	108.78	5.08	50.10	90.13	2.23	26.65
PT	481.83	5.92	13.26	134.07	3.79	29.24	122.76	4.77	40.64	100.02	4.38	45.27

Table 6 Normalized evaluation matrix

Sp.code	C1	C2	C3	C4	C5	C6	C7	C8	C9	C10	C11	C12
SP	0.468	0.522	0.419	0.492	0.479	0.325	0.431	0.317	0.269	0.482	0.411	0.315
CR	0.303	0.245	0.326	0.271	0.436	0.544	0.424	0.437	0.394	0.339	0.283	0.317
EL	0.316	0.358	0.434	0.283	0.358	0.429	0.322	0.297	0.327	0.358	0.270	0.277
SQ	0.417	0.346	0.309	0.485	0.418	0.290	0.330	0.310	0.341	0.310	0.341	0.399
HX	0.363	0.388	0.393	0.274	0.354	0.447	0.417	0.341	0.306	0.270	0.361	0.496
PL	0.371	0.365	0.378	0.475	0.325	0.236	0.330	0.466	0.524	0.399	0.298	0.286
PT	0.383	0.370	0.370	0.260	0.215	0.274	0.373	0.437	0.425	0.443	0.586	0.486

6. Technique for order of preference by similarity to ideal solution

In this study, the conversion of multi response criteria as a single response is employed using the TOPSIS technique. The significance of TOPSIS is effective conversion of multi-objective in to single objective and in view of choosing best alternative parameter which is to be mainly based on closeness coefficient values. Here, it is hypothesized for deriving positive ideal alternative which possess the best level for all attributes involved and negative ideal alternative termed for the worst level. The various steps involved in formulating multi objective characteristics involving TOPSIS are follows. The initial step is to arrange the response variables in matrix form.

$$D_M = \begin{pmatrix} q_{11}\ q_{12}\ q_{13} \cdots & \cdots q_{1n} \\ q_{12}\ q_{22}\ q_{23} \cdots & \cdots\ q_{2n} \\ q_{13}\ q_{32}\ q_{33} \cdots & \cdots\ q_{3n} \\ \cdots\ \ \cdots\ \ \cdots\ \ddots & \ddots\ \ \cdots \\ \cdots\ \ \cdots\ \ \cdots\ \ddots & \ddots\ \ \cdots \\ q_{m1} q_{m2} q_{m3} \cdots & \cdots\ q_{mn} \end{pmatrix} \tag{8}$$

Where q_{ij} is the performance of i_{th} alternative in relation to the j_{th} attribute.

In the current study, there are 7 alternatives (Patterned tubes as shown in Fig. 2) and 12 criteria (P_{max}, EA and CFE) as depicted which form the evaluation matrix (D_M) as shown in Table 5, in which each entry, (a_{ij}), may be the value assigned for alternative (i) with respect to the criterion (j).

The second step is the normalization of decision matrix by employing the following equation

$$r_{ij} = \frac{a_{ij}}{\sqrt{\sum_{i=1}^{m} q_{ij}^2}} \quad j=1,2,3\ldots n \tag{9}$$

Where i=1……m and j-1…..n, (a_{ij}) express the actual values of the ith value of the performed experiment no j (Palanivelu *et al*. 2011). r_{ij} stands for the entry of normalized evaluation matrix, R, as expressed bold in Table 6. The criteria which are to be evaluated have been renamed as C1~C12 for achieving clarity, which is normally corresponding to the same column as shown in Table 5.

The third step is performed by multiplying the normalized decision matrix to its corresponding weights and the weighted normalized decision matrix is shown as

$$V = w_{ij} r_{ij} \tag{10}$$

Where $\sum_{j=1}^{n} w_j = 1$

Where i=1……m and j-1…..n, w_j represents the weightage of j_{th} attribute.

In our present case, all the criteria's involved possess same weight. The current step may be skipped because it had no effect regarding to the final score obtained on each patterned tubes.

The fourth step is to determine the positive ideal solution (PIS) and negative ideal solution (NIS) by using the following formulas

$$V^+ = \left\{ \left(\sum_i^{max} U_{ij}\ |j \in J \right) \left(\sum_i^{min}\ |j \in J| i = 1,2 \cdots m \right) \right\} \tag{11}$$

$$= \{\ v_1^+, v_2^+, \ldots\ldots v_n^+ \}$$

Table 7 Ideal and negative ideal alternative

	C1	C2	C3	C4	C5	C6	C7	C8	C9	C10	C11	C12
A+	0.303	0.522	0.434	0.260	0.479	0.544	0.322	0.466	0.524	0.270	0.586	0.496
A-	0.468	0.245	0.309	0.492	0.215	0.236	0.431	0.297	0.269	0.482	0.270	0.277

Table 8 Obtained values of D^+ and D^- of each alternative

Sp.code	D^+	D^-
SP	0.580	0.434
CR	0.493	0.527
EL	0.896	0.428
SQ	0.944	0.349
HX	1.035	0.505
PL	1.043	0.390
PT	0.468	0.523

Table 9 Obtained score and ranking in TOPSIS

Sp.code	Score	Normalised value of TOPSIS	Ranking
SP	0.428	0.160	3
CR	0.517	0.194	2
EL	0.323	0.121	5
SQ	0.270	0.101	7
HX	0.328	0.123	4
PL	0.272	0.102	6
PT	0.528	0.198	1

$$V^+ = \left\{\left(\sum_i^{min} U_{ij} \mid j \in J\right)\left(\sum_i^{max} \mid j \in J \mid i = 1,2 \cdots m\right)\right\} \quad (12)$$

$$= \{ v_1^-, v_2^-, \dots \dots v_n^-\}$$

Here both ideal and negative ideal alternatives can be obtained from the matrix R which is shown in Table 7. The lowest initial peak force, larger energy absorption and crash force efficiency is termed for ideal alternative (A^+). The highest initial peak force, lowest energy absorption and crash force efficiency is termed for negative ideal alternative (Estrada *et al*. 2016). The elapsed distance of the i_{th} alternative with respect to the ideal/negative ideal alternative, it can be designated by

$$D_i^+ = \sqrt{\sum_{j=1}^{12}\left(V_{ij} - V_j^+\right)^2}, \quad i = 1,2, \dots i \quad (13)$$

$$D_i^- = \sqrt{\sum_{j=1}^{12}\left(V_{ij} - V_j^-\right)^2}, \quad i = 1,2, \dots i \quad (14)$$

The obtained values of D^+ and D^- of each alternative are shown in Table 8.

Finally, the closeness coefficient for each alternative is calculated by using the equation

$$S_i^+ = \frac{D_i^-}{D_i^+ + D_i^-} \quad (15)$$

Here, S_i^+represents the closeness coefficient of the i_{th} alternative. The obtained value of $S^+$for each alternative is illustrated in Table 9. The better alternative has S^+value closer to 1. Finally, normalized values of TOPSIS are achieved and ranking is done based on the above. The ranking indicates that patterned tubes with Pentagon (PT) and circle (Pellettiere *et al.*) cut-outs experiences highest score while the square (SQ) cut-outs achieves the lowest.

7. Conclusions

The crashworthiness indicators of tubes with patterned windows of various shapes along with the simple tubes were examined analytically and experimentally under axial and oblique loading conditions. The FE codes ABAQUS/Explicit were employed in developing the numerical model. In order to validate the developed numerical model, the experiment on the axial quasi-static loading of tubes (simple and windowed) at 0° inclination was performed. Comparison between the absorbed energy, collapse modes and progression, mean and maximum force exhibits that the numerical results are in good agreement with the experimental data. Followed by, the quasi-static loading of the model was performed at different load angles. The result reveals that the crashworthiness indices are better for windowed tubes comparing on par with simple tubes.

- The windowed tubes with various profiles (SP, CR, EL and HX) experiences complete diamond mode irrespective of all load angles (θ=0°, 10°, 20° and 30°). The mixed mode in which involves both concertina & diamond for the profile (PT) and complete concertina mode is observed for the profile (PL) for all load angles.
- The cross sectional shape of the pattern had drastically influences the energy absorbing ability and buckling behavior of the windowed tubes. The simple tubes experiences higher energy absorption rate at the AOI (10 and 20°) as 8.35 and 8.44 J. The higher energy absorption rate had significantly increases the peak force which in turn reduces the CFE values about 14.99% and 34.69% for the above AOI. The drastic reduction of energy absorption rate is experienced for AOI (20 and 30°) as 3.46 and 3.08 J. Even though energy absorption rate is reduced, the rise in CFE values of 25.73% and 29.29% is observed.
- The lowest CFE is recorded under axial loading is about 11.07 for square tubes and the highest being 15.53 for the Ellipse-hole profile tube. It is evident that lesser CFE is achieved in axial loading (θ=0°) due to the formation of progressive diamond collapse mode provokes high peak (P_{max}) load carrying capacity on par compare to the mean load (P_{mean}).
- The obtained value indicates that the presence of

geometric imperfections in the tubes had significantly increases the energy absorbing ability, while comparing with the windowed tubes with the simple tubes. Also, the lowest initial peak force was observed in windowed tubes than that of simple tubes and the tubes with circular windows are very effective in lowering initial peak load.

Lastly, the overall performance on crushing responses are assessed with the TOPSIS method on considering the criteria as initial peak, energy absorption and crash force efficiency. The highest score was exhibited for pentagonal and circular windowed tubes, while the square tubes have the least ranking. Finally, the results have proven that the crushing response of the tubes can improvise by introducing windowed shapes effectively and it also reveals pentagon and circular are the best window cut-outs.

References

ABAQUS, V (2011), *6.10. 3 Documentation*, Dassault Systems.

Abdul-Latif, A., Ahmed-Ali, A., Baleh, R. and Ouali, M.O. (2017), "Innovative solution for strength enhancement of metallic like-composite tubular structures axially crushed used as energy dissipating devices", *Thin-Wall. Struct.*, **119**, 332-344.

Altenhof, W., Powell, C., Harte, A.M. and Gaspar, R. (2005), "An experimental investigation into the energy absorption and force/displacement characteristics of aluminum foam filled braided stainless steel tubes under quasistatic tensile loading conditions", *Int. J. Crashworth.*, **10**(1), 21-31.

Altin, M., Acar, E. and Güler, M. (2018), "Foam filling options for crashworthiness optimization of thin-walled multi-tubular circular columns", *Thin-Wall. Struct.*, **131**, 309-323.

An, X., Gao, Y., Fang, J., Sun, G. and Li, Q. (2015), "Crashworthiness design for foam-filled thin-walled structures with functionally lateral graded thickness sheets", *Thin-Wall. Struct.*, **91**, 63-71.

Arnold, B. and Altenhof, W. (2004), "Experimental observations on the crush characteristics of AA6061 T4 and T6 structural square tubes with and without circular discontinuities", *Int. J. Crashworthv*, **9**(1), 73-87.

Auersvaldt, R.R. and Alves, M. (2014), "Impact behavior of windowed polygonal tubes", *Proceedings of the Iternational Conference on Advances in Civil, Strucutural and Mechanical Engineering*.

Baaskaran, N., Ponappa, K. and Shankar, S. (2017), "Quasi-static crushing and energy absorption characteristics of thin-walled cylinders with geometric discontinuities of various aspect ratios", *Lat. Am. J. Sol. Struct.*, **14**(9), 1767-1787.

Baaskaran, N., Ponappa, K. and Shankar, S. (2018), "Assessment of dynamic crushing and energy absorption characteristics of thin-walled cylinders due to axial and oblique impact load", *Steel Compos. Struct.*, **28**(2), 179-194.

Børvik, T., Hopperstad, O., Reyes, A., Langseth, M., Solomos, G. and Dyngeland, T. (2003), "Empty and foam-filled circular aluminium tubes subjected to axial and oblique quasistatic loading", *Int. J. Crashworth.*, **8**(5), 481-494.

Chen, W. and Wierzbicki, T. (2001), "Relative merits of single-cell, multi-cell and foam-filled thin-walled structures in energy absorption", *Thin-Wall. Struct.*, **39**(4), 287-306.

Cheng, Q., Altenhof, W. and Li, L. (2006), "Experimental investigations on the crush behaviour of AA6061-T6 aluminum square tubes with different types of through-hole discontinuities", *Thin-Wall. Struct.*, **44**(4), 441-454.

Dehghan-Manshadi, B., Mahmudi, H., Abedian, A. and Mahmudi, R. (2007), "A novel method for materials selection in mechanical design: Combination of non-linear normalization and a modified digital logic method", *Mater. Des.*, **28**(1), 8-15.

DeRuntz, J.A. and Hodge, P. (1963), "Crushing of a tube between rigid plates", *J. Appl. Mech.*, **30**(3), 391-395.

Eboreime, O., Ali, M., Kraft, F. and Alam, K. (2018), "Development of aluminum alloy 6063 T6 and T7 material models and their effects on energy-absorbing characteristics of cross-axial members", *J. Strain Analy. Eng. Des.*, **53**(4), 266-281.

Estrada, Q., Szwedowicz, D., Baltazar, M., Cortes, C., Majewski, T. and Estrada, C.A. (2016), "The performance of energy absorption in structural profiles with different discontinuities", *Int. J. Adv. Manufact. Technol.*, **84**(5-8), 1081-1094.

Estrada, Q., Szwedowicz, D., Majewski, T., Oliver, M., Cortes, C. and Castro, F. (2017), "Effect of discontinuity size on the energy absorption of structural steel beam profiles", *Mech. Adv. Mater. Struc.*, **24**(1), 88-94.

Estrada, Q., Szwedowicz, D., Silva-Aceves, J., Majewski, T., Vergara-Vazquez, J. and Rodriguez-Mendez, A. (2017), "Crashworthiness behavior of aluminum profiles with holes considering damage criteria and damage evolution", *Int. J. Mech. Sci.*, **131**, 776-791.

Fan, Z., Lu, G. and Liu, K. (2013), "Quasi-static axial compression of thin-walled tubes with different cross-sectional shapes", *Eng. Struct.*, **55**, 80-89.

Ferdynus, M. (2013), "An energy absorber in the form of a thin-walled column with square cross-section and dimples", *Eksploatacja i Niezawodność*, **15**(3), 253-258.

Ferdynus, M, Kotełko, M. and Kral, J. (2018), "Energy absorption capability numerical analysis of thin-walled prismatic tubes with corner dents under axial impact numeryczna analiza energochłonności cienkościennych słupów pryzmatycznych z przetłoczeniami", *Eksploatacja i Niezawodnosc*, **20**(2), 252.

Gautam, S.S. and Dixit, P. (2012), "Numerical simulation of ductile fracture in cylindrical tube impacted against a rigid surface", *Int. J. Dam. Mech.*, **21**(3), 341-371.

Ghamarian, A., Zarei, H., Farsi, M. and Ariaeifar, N. (2013), "Experimental and numerical crashworthiness investigation of the empty and foam-filled conical tube with shallow spherical caps", *Strain*, **49**(3), 199-211.

Guler, M.A., Cerit, M.E., Bayram, B., Gerceker, B. and Karakaya, E. (2010), "The effect of geometrical parameters on the energy absorption characteristics of thin-walled structures under axial impact loading", *Int. J. Crashworth.*, **15**(4), 377-390.

Huang, X., Lu, G. and Yu, T.X. (2002), "On the axial splitting and curling of circular metal tubes", *Int. J. Mech. Sci.*, **44**(11), 2369-2391.

Hwang, C.L., Lai, Y.J. and Liu, T.Y. (1993), "A new approach for multiple objective decision making", *Comput. Operat. Res.*, **20**(8), 889-899.

Johnson, W. (1978), "Metallic energy dissipating systems", *Appl. Mech. Rev.*, **31**, 277-288.

Khalkhali, A., Mostafapour, M., Tabatabaie, S.M. and Ansari, B. (2016), "Multi-objective crashworthiness optimization of perforated square tubes using modified NSGAII and MOPSO", *Struct. Multidiscipl. Optim.*, **54**(1), 45-61.

Kim, H.S. (2002), "New extruded multi-cell aluminum profile for maximum crash energy absorption and weight efficiency", *Thin-Walled Struct.*, **40**(4), 311-327.

Langseth, M. and Hopperstad, O. (1997), "Local buckling of square thin-walled aluminum extrusions", *Thin-Wall. Struct.*, **27**(1), 117-126.

Lee, D.W., Ma, Z.D. and Kikuchi, N. (2011), "FOA (first-order-analysis) model of an expandable lattice structure for vehicle crash energy absorption of an inflatable morphing body", *Struct. Eng. Mech.*, **37**(6), 617-632.

Lesuer, D. (1999), *Experimental Investigation of Material Models for Ti-6Al-4V and 2024-T3*, University of California, Lawrence Livermore National Laboratory, Livermore, California, U.S.A.

Mamalis, A., Manolakos, D., Ioannidis, M. and Papapostolou, D. (2004), "Crashworthy characteristics of axially statically compressed thin-walled square CFRP composite tubes: experimental", *Compos. Struct.*, **63**(3-4), 347-360.

Marzbanrad, J., Abdollahpoor, A. and Mashadi, B. (2009), "Effects of the triggering of circular aluminum tubes on crashworthiness", *Int. J. Crashworth.*, **14**(6), 591-599.

Morris, A. (1971), "Experimental investigation into the effects of indenting a cylindrical shell by a load applied through a rigid boss", *J. Mech. Eng. Sci.*, **13**(1), 36-46.

Nikkhah, H., Guo, F., Chew, Y., Bai, J., Song, J. and Wang, P. (2017), "The effect of different shapes of holes on the crushing characteristics of aluminum square windowed tubes under dynamic axial loading", *Thin-Wall. Struct.*, **119**, 412-420.

Palanivelu, S., Van Paepegem, W., Degrieck, J., De Pauw, S., Vantomme, J., Wastiels, J., Kakogiannis, D. and Van Hemelrijck, D. (2011), "Low velocity axial impact crushing performance of empty recyclable metal beverage cans", *Int. J. Imp. Eng.*, **38**(7), 622-636.

Pellettiere, J.A., Crocco, J. and Jackson, K.E. (2011), "Rotorcraft full spectrum crashworthiness and occupant injury requirements", *Proceedings of the 67th American Helicopter Society, Forum*, Virginia, U.S.A., May.

Qiu, N., Gao, Y., Fang, J., Feng, Z., Sun, G. and Li, Q. (2015), "Crashworthiness analysis and design of multi-cell hexagonal columns under multiple loading cases", *Fin. Elem. Analy. Des.*, **104**, 89-101.

Song, J., Chen, Y. and Lu, G. (2012), "Axial crushing of thin-walled structures with origami patterns", *Thin-Wall. Struct.*, **54**, 65-71.

Song, J., Chen, Y. and Lu, G. (2013), "Light-weight thin-walled structures with patterned windows under axial crushing", *Int. J. Mech. Sci.*, **66**, 239-248.

Tarlochan, F., Samer, F., Hamouda, A., Ramesh, S. and Khalid, K. (2013), "Design of thin wall structures for energy absorption applications: Enhancement of crashworthiness due to axial and oblique impact forces", *Thin-Wall. Struct.*, **71**, 7-17.

Taştan, A., Acar, E., Güler, M. and Kılınçkaya, Ü. (2016), "Optimum crashworthiness design of tapered thin-walled tubes with lateral circular cutouts", *Thin-Wall. Struct.*, **107**, 543-553.

Toda, S. (1983), "Buckling of cylinders with cutouts under axial compression", *Exper. Mech.*, **23**(4), 414-417.

Wang, P., Zheng, Q., Fan, H., Sun, F., Jin, F. and Qu, Z. (2015), "Quasi-static crushing behaviors and plastic analysis of thin-walled triangular tubes", *J. Constr. Steel Res.*, **106**, 35-43.

Wu, X., Zhang, Q., Gu, B. and Sun, B. (2017), "Influence of temperature and strain rate on the longitudinal compressive crashworthiness of 3D braided composite tubes and finite element analysis", *Int. J. Dam. Mech.*, **26**(7), 1003-1027.

Zhang, X., Cheng, G. and Zhang, H. (2006), "Theoretical prediction and numerical simulation of multi-cell square thin-walled structures", *Thin-Wall. Struct.*, **44**(11), 1185-1191.

CC